Three-dimensional modeling of microwave discharges in a waveguide-based plasma source with experimental comparison

Wencong Zhang,[1] Li Wu,[2] Junwu Tao,[3] and Huacheng Zhu[2,*]

[1]*School of Electronics and Information Engineering, Guiyang University, 550005 Guiyang, People's Republic of China*
[2]*IAEM (Institute of Applied ElectroMagnetics), College of Electronics and Information Engineering,*
Sichuan University, 610065 Chengdu, People's Republic of China
[3]*LAPLACE (Laboratoire Plasma et Conversion d'Energie), INPT-ENSEEIHT, University of Toulouse,*
31071 Toulouse, France

This paper proposes a transient three-dimensional model to simulate microwave-induced discharges in a waveguide-based plasma source under intermediate pressures. A plane-symmetric simplification method is applied to simplify half of the microwave plasma source in the calculation domain, dramatically reducing the demand for computational resources and calculation time. Meanwhile, the numerical simulations remain in three dimensions without dimensionality reduction, which allows us to directly calculate the efficiency of power coupling from the incident microwave to the plasma. Besides, the computation decrease improves the convergence performance of the mathematical model, making it possible to model the entire discharge process from 1×10^{-9} to 1×10^4 s. This period covers the instantaneous microwave breakdown to the formation of a stable plasma column near steady state. The results have revealed the electromagnetic waveguide structure change of the microwave plasma source during the discharge process. Several microwave power-coupling efficiencies of the waveguide-based plasma source with different thicknesses and permittivities of the glass tube are calculated and compared with the experimentally measured data. Furthermore, the effects of the glass tube on the electromagnetic modes of the traveling microwave propagating along the plasma column and the discharge properties are also investigated. The numerically obtained results generally agree with the theoretical analysis and the experimental data in our previous studies, demonstrating the validity of the proposed mathematical model and the plane-symmetric simplification method.

I. INTRODUCTION

Microwave plasma sources (MPSs) [1–5], as one of the most popular plasma sources, have demonstrated outstanding potential in a wide range of applications such as material processing [6,7], hydrogen production [8–11], carbon dioxide elimination [12–15], waste disposal [16,17], and so on. Along with their increasing popularity, the demand for numerical analysis of discharge properties and microwave propagation characteristics in MPSs has increased dramatically in the last few decades. However, the mathematical model of MPSs is a highly nonlinear and strongly coupled equation system that greatly limits the iteration step and severely stretches the run-time. Moreover, because of the large gradients of the particle number densities in plasma, modeling the MPSs in two or three dimensions generally requires a dense mesh structure with a considerably large number of mesh cells, resulting in a huge matrix. Therefore, multidimensional modeling of the gas discharges in MPSs remains a formidable undertaking, which has high demands on both time and computational resources [18,19].

In fact, to the authors' knowledge, only a few numerical simulations have been conducted to model the discharges in MPSs, especially in two or three dimensions. To name some typical ones, Moisan and co-workers proposed a two-dimensional axisymmetric model in 2007 to investigate the discharge phenomenon and wave propagation in a surfaguide MPS at 915 MHz, which first considered the gas-flow effects [20]. In 2011, Tatarova utilized a similar two-dimensional axisymmetric model combined with the Boltzmann equation, having simulated the discharge of a nitrogen-argon mixture gas in an MPS under atmospheric pressure [21]. In 2013, Nowakowska modeled a waveguide-based MPS operating at a very high gas-inflow rate with the plasma fluid model in two dimensions [22]. In 2016, Georgieva compared the classic drift-diffusion approximation and the simplified ambipolar diffusion approximation in modeling the discharges in an MPS at intermediate pressures [23]. In 2018, Baeva established a new two-dimensional model based on the fluid method to simulate the argon plasmas under atmospheric pressure in a waveguide-based MPS and compared the results from three-dimensional simulations [24]. In 2017, our team proposed a two-dimensional axisymmetric fluid model to study the traveling wave formation and the plasma column maintenance in an MPS with metallic walls surrounding the dielectric tube operating at 2.45 GHz [25]. Furthermore, we improved the two-dimensional axisymmetric model, having investigated the gas-flow effects on the discharge properties and the microwave propagation characters in a two-port type MPS [26].

*Corresponding author: hczhu@scu.edu.cn

The above two-dimensional models [20–23,25,26], except the one in Ref. [24], have all utilized the axisymmetric simplification of the discharge tube (referred to the axis of the cylindrical discharge tube). It assumed azimuthal symmetry for the electromagnetic field in the discharge tube and only considered the cylindrical discharge tube in the calculation domain, while the rectangular waveguide part was neglected. Such a simplification can save a great deal of computational time and resources, allowing us to obtain informative insights about the MPSs with an acceptable calculation time and limited computational resources. However, the axisymmetric simplification also introduced two limitations. The two-dimensional model is no longer valid when the distribution of the traveling microwave in the discharge tube is not azimuthally symmetric. This case exists when the MPS has a glass tube with a thin wall and a large inner diameter [27]. Another limitation is the disability to calculate the microwave power reflection of the MPSs, because of the absence of the rectangular waveguide part in simulations. In other words, the two-dimensional axisymmetric model cannot be used to calculate the efficiency of power coupling from the incident microwave to the plasma.

This paper proposes a three-dimensional model based on the plasma fluid model to simulate the discharges and the microwave propagation in a waveguide-based MPS with a plane-symmetric simplification to the calculation domain. This model can overcome the limitations of the two-dimensional axisymmetric model, having a broader scope of validity and being able to estimate the microwave power coupling efficiency of the MPSs. Besides, compared with a complete three-dimensional model, the proposed plane-symmetric model halves the calculation domain and has a better convergence performance. The numerical results are compared with experimental results to validate the proposed three-dimensional model and the plane-symmetric simplification method.

II. MATHEMATICAL MODEL

A. Geometrical model and computational domain

Figure 1(a) shows the structure of an MPS based on a WR430 rectangular waveguide working at the microwave frequency of 2.45 GHz [1]. The discharge occurred in a quartz glass tube located at the center of the height-reduced rectangular waveguide and pierced through it. The glass tube parts out of the rectangular waveguide are enclosed by an upper and a lower pair of metal tubes with an inner diameter of 30 mm. It is worth noting that the metal tubes that shield the glass tube make the MPS differ from the microwave plasma torch proposed by Uhm *et al.* [2]. Besides. there is no air gap between the metal and the glass tubes, which is also slightly distinct from the classic surfaguide MPS proposed by Moisan [1]. The height of the glass tube is 200 mm. As for other detailed geometrical sizes of the MPSs, they can be found in our previous work [28]. Figure 1(b) gives the simplified calculation domain based on the plane-symmetric simplification method. Only half of the MPS structure is taken into the simulations ($x \leqslant 54.6$ mm), which can significantly reduce the calculation demand and the computational time.

The plane-symmetric simplification assumes that the microwave field and the plasma properties in the MPS are plane symmetric. The rectangular waveguide part of the MPS, including the standard waveguide WR430, the tapered waveguide, and the height-reduced part, allows the microwave at the frequency of 2.45 GHz to propagate only in TE_{10} mode. For the cylindrical discharge tube part of the MPS, it was demonstrated in our previous study that the traveling microwave sustaining the discharge could propagate either in a pure TEM mode or hybrid TE_{11} and TEM modes [27]. For these electromagnetic modes, the tangential component of the magnetic fields and the normal component of the electric fields in the plane across the tube length and the middle of the rectangular waveguide ($x = 54.6$ mm, as shown in Fig. 1) are zero. In other words, the electric field vector in the plane is parallel to it, while the magnetic field vector is perpendicular to it. In this case, the computational domain can be cut in half along the symmetric plane; an equivalent perfect magnetic conductor (PMC) boundary can be imposed on the plane. With this boundary, only a half of the MPS structure is needed in the calculation domain. In microwave numerical modeling, imposing a PMC boundary inside a microwave component to reduce the calculation domain is a commonly used skill [29]. It can be applied when the microwave device has a symmetric geometrical structure and a symmetric electric field distribution. As for the discharges in the MPS, the microwave distribution in the discharge tube can significantly determine the plasma properties, especially at low pressures. Therefore, assuming plane symmetry for the plasma in the MPS in this study is reasonable since its sustaining microwave is plane symmetric (either TEM or TE_{11} mode).
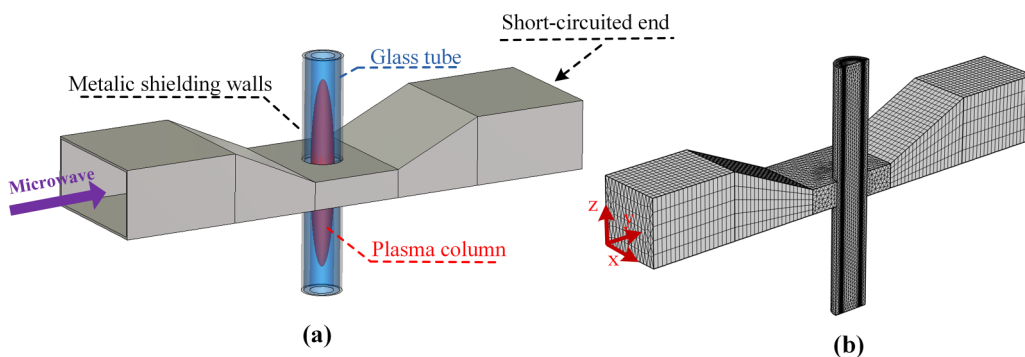

FIG. 1. Schematic diagram of the MPS and its calculation domain: (a) structure chart, and (b) computational domain.

In conclusion, the plane-symmetric simplification is valid, providing that the microwave in the discharge tube propagating along the plasma column and sustaining the discharge has a plane-symmetric field distribution.

B. Governing equations and boundary conditions

The microwave electric field distribution $\overrightarrow{E_{EM}}$ in the MPS can be obtained by solving the Helmholtz equation in the frequency domain with proper boundary conditions:

$$\nabla \times \left(\mu_r^{-1}\nabla \times \vec{E}_{EM}\right) - k_0^2\left(\varepsilon_r - \frac{j\sigma}{\omega\varepsilon_0}\right)\vec{E}_{EM} = 0. \quad (1)$$

In the above equation, ω is the microwave angular frequency, ϵ_0 is the constant permittivity in the vacuum, and k_0 is the wave number in free space. σ, ε_r, and μ_r indicate the electromagnetic properties of materials, which are electric conductivity, relative permittivity, and relative permeability, respectively. The plasma generated in the MPS can be equivalently regarded as a conductive medium, and its conductivity σ_p can be expressed as follows [30]:

$$\sigma_p = \frac{n_e q^2}{m_e(v_m + j\omega)}. \quad (2)$$

n_e is the electron number density in the unit of $1 \cdot \mathrm{m}^{-3}$, v_m is the electron elastic collision frequency with neutrals, and q and m_e are the elementary charge and mass of a single electron, respectively.

Argon, a widely used plasma working gas, is chosen in our study for its simplicity. The plasma generated in the MPS is assumed to contain only atomic ions, electrons, excited atoms, and background neutrals. The number densities of electrons, ions, and metastable atoms are obtained by solving three continuity equations as follows:

$$\frac{\partial n_k}{\partial t} + \nabla \cdot \overrightarrow{\Gamma_k} = R_k. \quad (3)$$

n_k represents the number density of species k, $\overrightarrow{\Gamma_k}$ is the number density flux, and R_k is the corresponding source term dominated by the plasma chemistry. The index k indicates metastable neutral atoms Ars ($k = s$), atomic ions Ar+ ($k = i$), and electrons ($k = e$). The number density of the ground-state argon atom Ar ($k = n$) is estimated from the following expression (4). The contributions of other components to the total pressure are neglected because of their small proportions.

$$n_n = \frac{P}{K_B T}. \quad (4)$$

K_B is the Boltzmann constant, and P is the gas pressure in pascal. Ions, metastable atoms, and neutrals are assumed to share a common constant temperature $T = 1000$ K. Actually, the temperature of the heavy species mixture (T) is not constant and it has a nonuniform spatial distribution, requiring a heat-transfer equation to describe it. Besides, its value changes with the increase of the input microwave power and gas pressures. In the present study, such an assumption is to simplify the mathematical model, making it possible to be solved in three dimensions and to simulate the entire discharge process from 1×10^{-9} to 1×10^4 s. Besides, the heavy species temperature is assumed to be 1000 K because the input microwave power is low in the present study (200 W). The electron temperature T_e (unit: K) can be determined from the following energy conservation equation:

$$\frac{\partial}{\partial t}\left(\frac{3}{2}T_e K_B n_e\right) + \nabla \cdot \overrightarrow{\Gamma_{en}} + q\overrightarrow{E_{es}} \cdot \overrightarrow{\Gamma_e} = Q_{EM} - Q_{el} - Q_{\mathrm{inel}}. \quad (5)$$

$\overrightarrow{\Gamma_{en}}$ is the electron energy density flux, $\overrightarrow{\Gamma_e}$ is the electron number density flux, and $\overrightarrow{E_{es}}$ is the static electric field due to the space charge. $Q_{EM} = \frac{1}{2}\mathrm{Re}(\sigma_p\vec{E} \cdot \vec{E}^*)$ is the power density absorbed from the microwave dissipation. Q_{inel} is the total power density change of electrons from the inelastic collisions with heavy species. $Q_{el} = \frac{3}{2}n_e K_B \frac{2m_e}{m_{\mathrm{Ar}}}v_m(T_e - T)$ is the power density transferred from electrons to neutrals and ions via elastic collisions. The static electric field $\overrightarrow{E_{es}}$ due to gas ionization and space charge is governed by Gauss' law as follows:

$$\nabla \cdot (\varepsilon_0\overrightarrow{E_{es}}) = \nabla \cdot (-\varepsilon_0\nabla V) = q(n_i - n_e). \quad (6)$$

V is the electric potential. For the number density fluxes of electrons and ions ($\vec{\Gamma}_e$ and $\vec{\Gamma}_i$), the classic drift-diffusion approximation is applied as follows:

$$\overrightarrow{\Gamma_e} = -n_e\mu_e\overrightarrow{E_{es}} - D_e\nabla n_e. \quad (7)$$

$$\overrightarrow{\Gamma_i} = n_i\mu_i\overrightarrow{E_{es}} - D_i\nabla n_i. \quad (8)$$

For the excited atoms, the number density flux $\overrightarrow{\Gamma_s}$ is determined by Fick's law as follows:

$$\overrightarrow{\Gamma_s} = -D_s\nabla n_s. \quad (9)$$

In the above equations, μ_e and μ_i are the mobilities of electrons and ions, respectively. D_e, D_i, and D_s are the diffusivities of electrons, ions, and excited atoms, respectively. Their values can be found in Ref. [31]. The flux of electron energy $\overrightarrow{\Gamma_{en}}$ can be described as follows:

$$\overrightarrow{\Gamma_{en}} = -\frac{5}{3}\mu_e\left(\frac{3}{2}T_e K_B n_e\right)\overrightarrow{E_{es}} - \frac{5}{3}D_e\nabla\left(\frac{3}{2}T_e K_B n_e\right). \quad (10)$$

The plasma mixture is assumed to consist of electrons, atomic ions Ar$^+$ (energy level: 15.7 eV), metastable atoms Ars (energy level: 11.56 eV), and ground-state neutrals Ar. It is worth noting the Ar_2^+ is overlooked in the present study as a compromise to complete the three-dimensional simulations. In fact, considering the molecular ion (Ar_2^+) in simulations definitely can increase the accuracy, as in our previous works and others [20,23–26,33]. However, the addition of Ar_2^+ would significantly increase the complexity of the equation system and the nonlinear couplings between each equation, leading to an unacceptable runtime and even the convergence failure for the three-dimensional model. Besides, the small difference between them results from the two-dimensional axisymmetric models with and without the Ar_2^+, indicating it is reasonable to waive the Ar_2^+ as a last resort for the three-dimensional model.

TABLE I. Reactions used in this model. The reaction rates for processes No. 6 and No. 7 have the unit of m^6/s. Other reaction rates have the unit of m^3/s.

No.	Reaction	Reaction rate	$\Delta\varepsilon_j$ [eV]	Reference
1	$e + Ar \Rightarrow e + Ars$	$4.9 \times 10^{-15}(T_e[eV])^{0.5}\exp(\frac{-11.65}{T_e[eV]})$	11.65	[32,33,20]
2	$e + Ars \Rightarrow e + Ar$	$4.8 \times 10^{-16}T_e^{0.5}[eV]$	−11.65	[32,33,20]
3	$e + Ar \Rightarrow 2e + Ar^+$	$1.27 \times 10^{-14}(T_e[eV])^{0.5}\exp(\frac{-15.76}{T_e[eV]})$	15.76	[32,33,20]
4	$e + Ars \Rightarrow 2e + Ar^+$	$1.37 \times 10^{-13}(T_e[eV])^{0.5}\exp(\frac{11.65-15.76}{T_e[eV]})$	4.11	[32,33,20]
5	$Ars + Ars \Rightarrow e + Ar + Ar^+$	6.2×10^{-16}	−7.54	[31,34]
6	$e + e + Ar^+ \Rightarrow e + Ars$	$8.75 \times 10^{-39}(T_e[eV])^{-4.5}$	−4.11	[35]
7	$e + Ar + Ar^+ \Rightarrow Ar + Ars$	$1.5 \times 10^{-40}(\frac{T[K]}{300})^{-2.5}$	−4.11	[36]
8	$e + Ar^+ \Rightarrow Ar + h\nu$	$2.174 \times 10^{-17}(T_e[eV])^{-0.5}$	−15.76	[36]
9	$Ar + Ar \Rightarrow Ars + Ar$	$1.68 \times 10^{-26}(T[K])^{1.5}(2 + \frac{135\,300}{T[K]})\exp(-\frac{135\,300}{T[K]})$		[36]
10	$Ars + Ar \Rightarrow Ar + Ar$	3×10^{-21}		[31,34]

According to Table I, the source terms of the continuity Eq. (3) can be written as follows:

$$R_e = R_i = k_3 n_e n_n + k_4 n_e n_s + k_5 n_s n_s - k_6 n_e n_e n_i$$
$$- k_7 n_e n_n n_i - k_8 n_e n_i, \tag{11}$$

$$R_s = k_1 n_e n_n - k_2 n_e n_s - k_4 n_e n_s - 2k_5 n_s n_s + k_6 n_e n_e n_i$$
$$+ k_7 n_e n_n n_i + k_9 n_n n_n - k_{10} n_s n_n. \tag{12}$$

The source term of the electron energy balance equation can be determined as shown in Eq. (13):

$$Q_{\text{inel}} = q \begin{pmatrix} 11.65k_1 n_e n_n - 11.65k_2 n_e n_s + 15.76k_3 n_e n_n + 4.11k_4 n_e n_s \\ -7.54k_5 n_s n_s - 4.11k_6 n_e n_e n_i - 4.11k_7 n_e n_n n_i - 15.76k_8 n_e n_i \end{pmatrix}. \tag{13}$$

C. Boundary conditions and initial values

For the Helmholtz equation, the normalized microwave excitation at the input port (at the *X0Z* plane as shown in Fig. 1) can be described by the following expression:

$$\overrightarrow{E_{0z}} = \overrightarrow{e_z} \sin\left(\pi \frac{x}{a}\right) e^{-j\beta y}. \tag{14}$$

$\beta = \frac{2\pi}{c}\sqrt{f^2 - \frac{c^2}{(2 \times a)^2}}$ is the phase constant of the microwave in the WR430 waveguide, where f is the frequency of the input microwave and c is the speed of light in the vacuum. $a = 0.1092$ (m) and $b = 0.0546$ (m) are the width and the height of the standard rectangular waveguide WR430, respectively. $\overrightarrow{E_{0z}}$ is the normalized z component of the microwave electric field on the cross section of the standard rectangular waveguide WR430, while other components ($\overrightarrow{E_{0x}}$ and $\overrightarrow{E_{0y}}$) are zero. Such field distribution characteristics accord with the TE$_{10}$ mode. With the normalized microwave electric field, the total input power can be obtained by calculating the integral of the Poynting vector on the cross section of the rectangular waveguide WR430. When the input microwave power increases to P_{in} (unit: W), the magnitude of the microwave electric field changes, and the z component of the microwave electric field $\overrightarrow{E_z}$ can be rewritten as follows:

$$\overrightarrow{E_z} = \overrightarrow{e_z} \frac{P_{\text{in}}}{\frac{1}{2}\text{Re}\oint_s (\overrightarrow{E_{EM}} \times \overrightarrow{H_{EM}^*}) \cdot d\overrightarrow{S}} \sin\left(\pi \frac{x}{a}\right) e^{-j\beta y}$$
$$= \overrightarrow{e_z} \frac{P_{\text{in}}}{\frac{ab}{4Z_{TE_{10}}}} \sin\left(\pi \frac{x}{a}\right) e^{-j\beta y}. \tag{15}$$

In the above equation, Re denotes the real part of the expression and $*$ indicates the complex conjugate. $\overrightarrow{H_{EM}}$ is the microwave magnetic field. S indicates the microwave input port at the *X0Z* plane, as shown in Fig. 1. $Z_{TE_{10}} = 120\pi/\sqrt{1 - [c/(2af)]^2}$ is the equivalent wave impedance of TE$_{10}$ mode. The perfect magnetic conductor boundary on the plane-symmetric surface, as shown in Fig. 1, can be described by the following equation:

$$\overrightarrow{e_n} \times \overrightarrow{H_{EM}} = 0. \tag{16}$$

$\overrightarrow{e_n}$ is the unit outward normal vector for the boundary. It assumes that the microwave entering the discharge tube (the glass tube, the plasma column, and their surrounding metallic shielding walls) will not be reflected. In other words, no backward microwave propagates from the ends of the discharge tube to the rectangular waveguide. In this case, a set of scattering boundary conditions, as shown in Eq. (17), are imposed on both ends of the discharge tube, enabling us to model the discharge tube with a finite height (200 mm in our case). Other boundaries for the Helmholtz equation are treated as perfect electric conditions (PEC).

$$\overrightarrow{e_n} \times \nabla \times \overrightarrow{E_{EM}} - jk\overrightarrow{e_n} \times (\overrightarrow{E_{EM}} \times \overrightarrow{e_n}) = 0. \tag{17}$$

For the electrostatic equation, the inner glass-tube wall is set to the electric reference ground $V = 0$, because all the charged particles are assumed to be not accumulated but quenched when they reach the inner glass-tube wall. Other boundaries for the electrostatic field are set to zero charge, $\overrightarrow{e_n} \cdot \vec{D} = 0$. For the continuity equations to describe the num-

ber densities of electrons, ions, and excited atoms, a set of Neumann boundary conditions are imposed on the inner glass-tube walls as shown in Eq. (18). The zero-flux boundary conditions ($\overrightarrow{e_n} \cdot \overrightarrow{\Gamma_k} = 0$) are enforced on other boundaries.

$$\overrightarrow{e_n} \cdot \overrightarrow{\Gamma_k} = \frac{1}{4} n_k \sqrt{\frac{8 K_B T_k}{\pi m_k}}. \qquad (18)$$

The boundary conditions of the electron energy density equation on the inner glass-tube walls can be described in Eq. (19). Other boundaries are specified as zero-flux boundary conditions ($\overrightarrow{e_n} \cdot \overrightarrow{\Gamma_{en}} = 0$).

$$\overrightarrow{e_n} \cdot \overrightarrow{\Gamma_{en}} = \frac{5}{2} K_B T_e \left(\frac{1}{4} n_e \sqrt{\frac{8 K_B T_e}{\pi m_e}} \right). \qquad (19)$$

The gas pressure P and the microwave input power P_{in} are set to 500 Pa, 1000 Pa, and 200 W, respectively, which are consistent with the experimental conditions (Fig. 2) [28]. To simulate the whole discharge process from microwave breakdown to the formation of a stable plasma, the initial value of the electron number density in the simulation of Figs. 3–5 is set to be 1×10^{15}/m^3. This value is lower than the critical number density at the microwave frequency of 2.45 GHz (7.6×10^{16}/m^3 corresponds to $\omega_P = \omega$ [25]), but relatively high to save computational time. Meanwhile, the initial values for ions and excited atoms are set to be 1×10^{15}/m^3 and 1×10^{13}/m^3, respectively. For other calculations in the present study, the initial values for electrons, ions, and excited atoms are specified as 1×10^{17}/m^3, 1×10^{17}/m^3, and 2.4×10^{13}/m^3, respectively, for a fast convergence. Besides, 2.67 eV is specified as the initial value of the electron temperature in all the calculations. Other values are also permitted if the computational resource is abundant enough and the convergence time is acceptable. The relative permittivity of the quartz glass tube (ε_g) is 3.5 (except see the simulations in Fig. 9).

D. Calculation procedure and numerical implementation

The mathematical model is time dependent, and its calculation procedure is shown in Fig. 2. This model can simulate the whole discharge process from the initial time at 1×10^{-9} s until 10 000 s tending to the steady state. Each calculation starts by solving the Helmholtz equation in the frequency domain. Then, it solves the energy conservation equation of electrons and the continuity equation for the number density of excited atoms in the transient domain and segregated steps. Afterwards, the continuity equations for the number densities of electrons and ions, the Poisson equation for electric potential, and its gradients for the electrostatic field are lumped together and solved in the transient domain. If the modeling time does not reach 10 000 s, the calculation turns back to solving the Helmholtz equation with the updated plasma conductivity and starting another loop in the next time step. The absolute and relative tolerances are set to 0.01 for each loop and calculation at all time steps.

The mathematical model and its numerical computation were implemented in a commercial computational suit named COMSOL MULTIPHYSICS, mainly with its partial differential
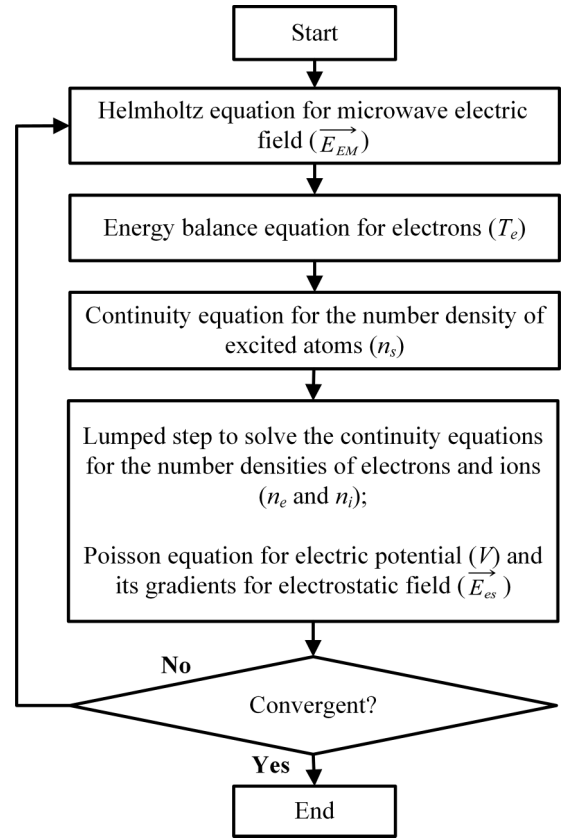

FIG. 2. Calculation procedure.

equation interface. The number of mesh elements changes with the thickness of the glass tube wall. However, it was validated by comparing the results with those from a much denser mesh structure. These calculations were run on a computer with 2 E5-2630V2 CPUs and 128 GB RAM. It took about 4–7 days to complete a calculation.

III. RESULTS AND DISCUSSION

A. Process of the microwave breakdown in the MPS

To better understand the obtained results, the field distributions in Figs. 3, 4, 6, and 7 are presented with a mirror-symmetry skill to show the complete configuration of the MPS. Figure 3 shows the variation of the electron number density distribution in the discharge process. It can be observed in Fig. 3 that the microwave breakdown occurs initially in the glass tube near the tube wall intersecting with the rectangular waveguide, where the waveguide height is compressed, and the microwave electric field intensity is enhanced. As time passes, the discharge area becomes increasingly long towards both ends of the glass tube and extends to the tube's axis. When the time reaches 1×10^{-3} s, the discharge tends to be stable, and the shape of the plasma column no longer changes over time.

Figure 4 presents the microwave electric field distribution change in the entire discharge process. At the beginning (1×10^{-9} s), the electron number density is 1×10^{15}/m^3, far smaller than the critical number density of 7.6×10^{16}/m^3. It indicates that the microwave at the frequency of 2.45
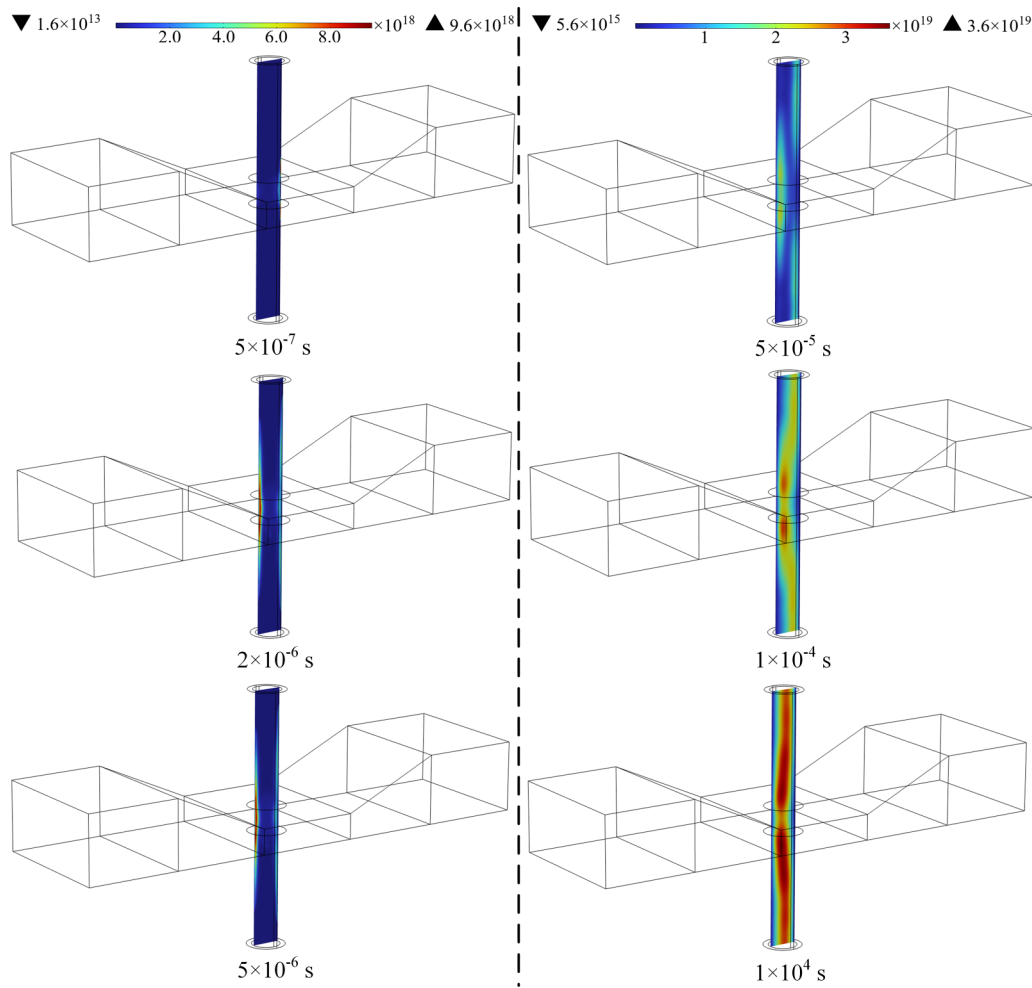
FIG. 3. Variation of the electron number density $(1/m^3)$ distribution at different times ($P = 1000$ Pa; $P_{in} = 200$ W; $D_g = 4$ mm; and $\varepsilon_g = 3.5$).
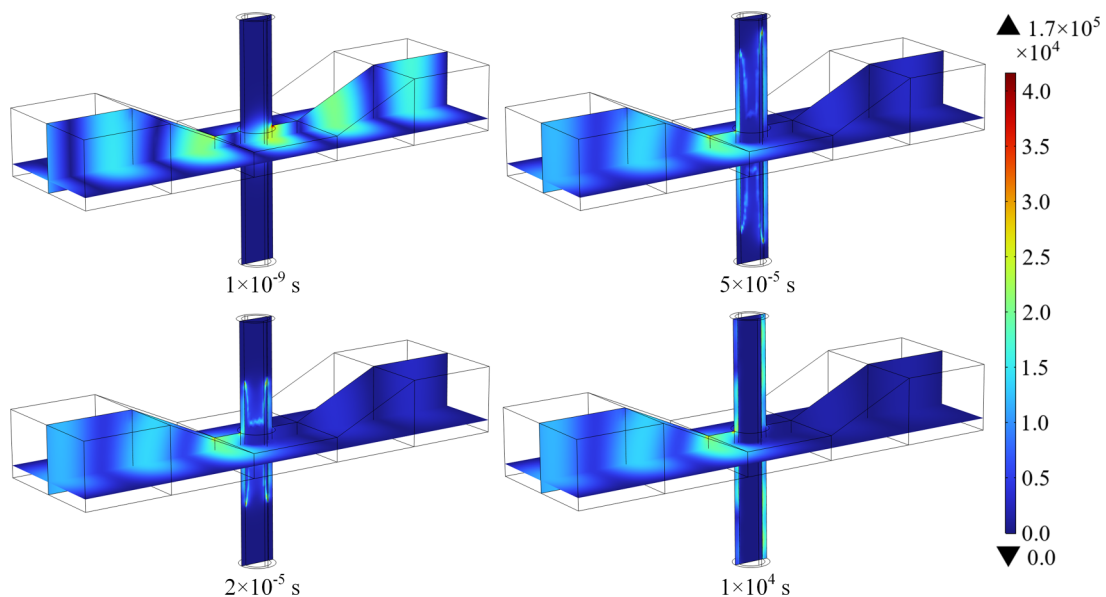

FIG. 4. Variation of the microwave electric field (V/m) distribution at different times ($P = 1000$ Pa; $P_{in} = 200$ W; $D_g = 4$ mm; and $\varepsilon_g = 3.5$).
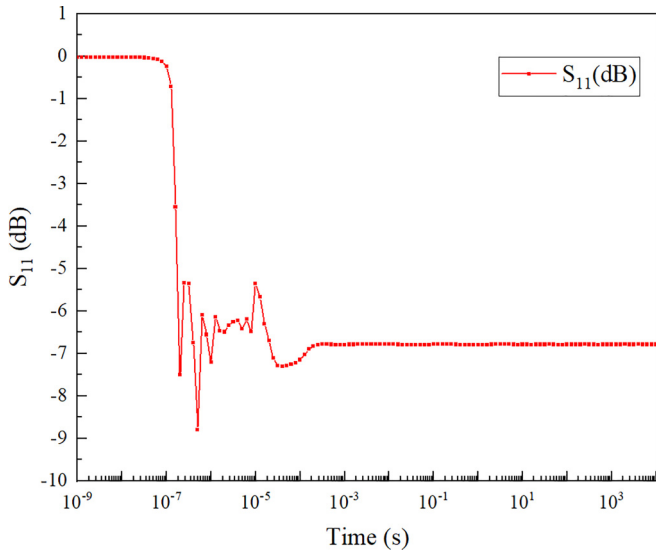
FIG. 5. Variation of the S_{11}(dB) parameter at different times ($P = 1000$ Pa; $P_{in} = 200$ W; $D_g = 4$ mm; and $\varepsilon_g = 3.5$).

GHz can penetrate the glass tube and the discharge area with little loss and reflection. Therefore, the microwave in the MPS is almost a pure standing wave only existing in the rectangular waveguide part, as shown in Fig. 4 (time = 1×10^{-9} s). When the microwave breakdown occurs in the glass tube and the electron number density exceeds 7.6×10^{16}/m^3, the conductive plasma will behave like a conductor that can shield the microwave from penetrating itself. The high-density plasma and its surrounding metallic walls can be regarded as a two-conductor waveguide with no cutoff-frequency limitation. Therefore, the incident microwave can enter the cylindrical discharge tube, propagating in the glass-tube wall along the plasma towards both ends of the tube. The traveling microwave dissipates in the plasma and drives the discharge area to extend when time passes, as shown in Fig. 4

(time = 2×10^{-5} and 5×10^{-5} s). When the discharge becomes stable, the traveling wave in the discharge tube will have a particular field distribution called electromagnetic modes that sustain the discharge and greatly influence the plasma properties.

Figure 5 gives the change of the S_{11}(dB) parameter of the MPS at different times, which shows the microwave energy dissipation in the whole discharge process. S_{11} is defined as the ratio of the reflected wave's voltage to the incident wave's voltage at the microwave input port, which can be also expressed in decibels (dB) in engineering. For the cases that microwave is incident from only one port of the MPS in present study, the smaller the S_{11} is, the higher the microwave power-coupling efficiency of the MPS will be. This is because microwave power can be either reflected or absorbed by the plasma in the one-port microwave excitation cases. When the electron number density is low at the beginning of the microwave breakdown, the plasma has a considerably weak wave-absorbing capability and nearly all the microwave power is reflected by the short-circuited end. Therefore, the S_{11}(dB) parameter is approximately equal to 0 dB at first, so the incident microwave power is almost reflected without dissipation. As time passes, the electron number density and the wave-absorbing capability of the plasma increase. However, when the electron number exceeds the critical density 7.6×10^{16}/m^3, the plasma becomes conductive enough and reflects the incident microwave power. Meanwhile, the waveguide structure of the MPS changes from a rectangular waveguide with two cutoff circular waveguides (the cylindrical discharge tube) to a waveguide-coaxial mode converter. The incident microwave power enters the discharge tube propagating along the plasma and dissipating in it. The S_{11}(dB) parameter can be approximately equal to -7 dB, indicating that about 20% of the incident microwave power is reflected (40 W when $P_{in} = 200$ W in our case). The drastic change of the S_{11}(dB) parameter from 1×10^{-7} to 1×10^{-4} s, as shown in Fig. 5, is because of the significant change of the electromagnetic wave
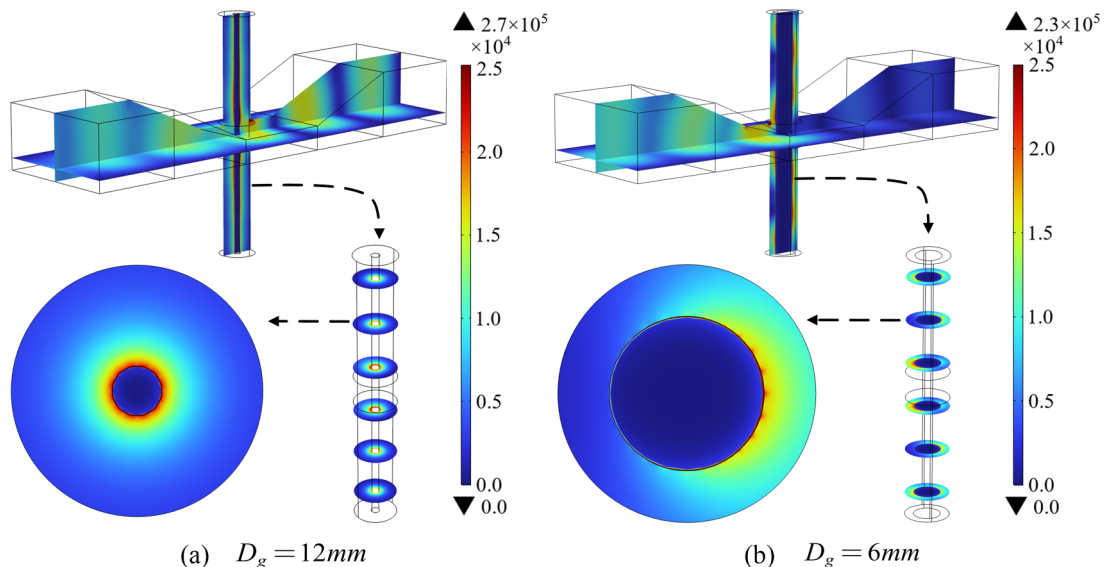

(a) $D_g = 12mm$

(b) $D_g = 6mm$

FIG. 6. Axisymmetric and nonaxisymmetric microwave electric fields (V/m) in the discharge tube. ($P = 1000$ Pa; $P_{in} = 200$ W; and $\varepsilon_g = 3.5$).

(a) Distributions of the microwave electric field (V/m)   (b) Distributions of the electron number density ($1/m^3$)
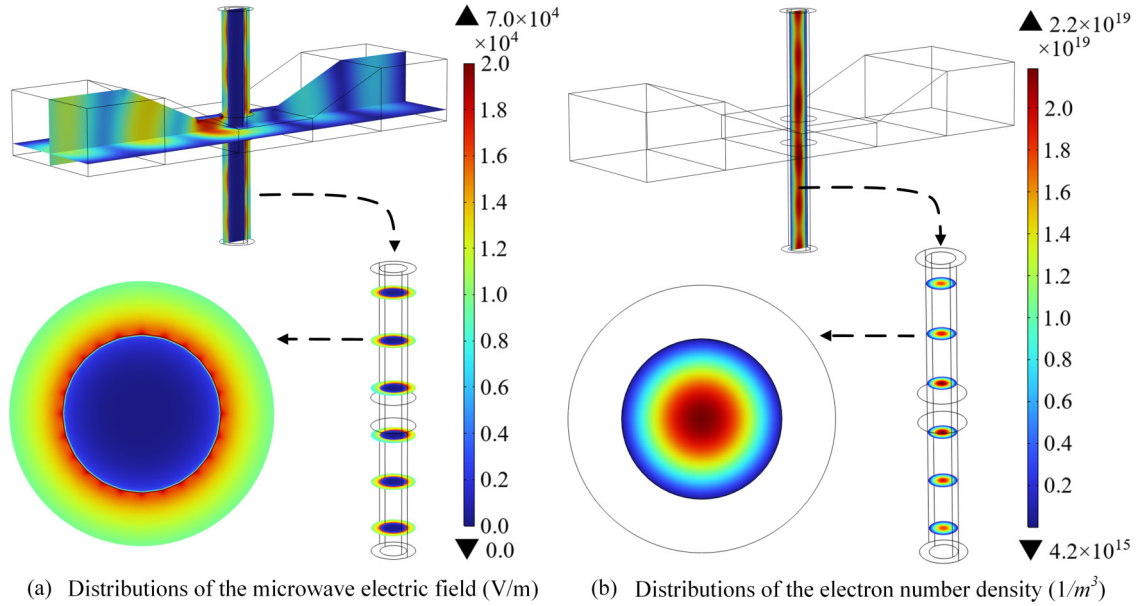
FIG. 7. Distributions of the microwave electric field (V/m) and the electron number density ($1/m^3$) in the MPS ($P = 1000$ Pa; $P_{in} = 200$ W; $D_g = 6$ mm; and $\varepsilon_g = 1.5$).

distribution in the discharge tube. This period is the time of the MPS waveguide structure transition. After 1×10^{-3}, the discharge turns stable, and the microwave power reflection becomes constant as well.

B. Efficiency of power coupling from the incident microwave to the plasma under different operation conditions

The microwave-induced discharges in the waveguide-based MPS under different operation conditions (glass tubes with different wall thicknesses and dielectric properties, different gas pressures) were modeled, and the corresponding S_{11} (dB) parameters near steady state at 10 000 s were calculated. Part of the numerical results is compared with the experimental data in our previous study [28] to evaluate the validity of the above mathematical model. Figure 8 presents the variation of the microwave power-coupling efficiency with the increase in the thickness of the glass-tube wall (D_g) from 1.5 to 10 mm, when the gas pressure is 1000 Pa and the input microwave power is 200 W. In all the calculations in the present study, the outer diameter of the glass tube remains 30 mm. That is, increasing the thickness of the glass-tube wall means the decrease of the discharge area. For the waveguide-based MPS with the incoming microwave from only one port, the efficiency of power coupling from the incident microwave to the plasma (η) can be calculated with the numerically obtained S_{11} parameter as follows:

$$\eta = 1 - |S_{11}|^2. \tag{20}$$

Here, the microwave energy radiated from both ends of the discharge tube is neglected, which may lead to overestimating the microwave power-coupling efficiency. However, the negligence is consistent with the assumption that there is no reflected microwave power at both ends of the discharge tube in the above paragraphs.

Compared with the experimental data, the numerical results have shown a similar change tendency that the microwave coupling efficiency improves when the thickness of the glass-tube wall enhances, although the change is not a strict monotonic increase. Besides, it indicates that an efficiency higher than 85% can be achieved by simply choosing a glass tube with proper wall thickness. These conclusions accord with the experiments in our previous study [28]. However, it is worth noting that the calculated microwave power-coupling efficiency does not perfectly match the measured data, especially when the thickness of the glass-tube wall is small. Besides the influence introduced by the limited
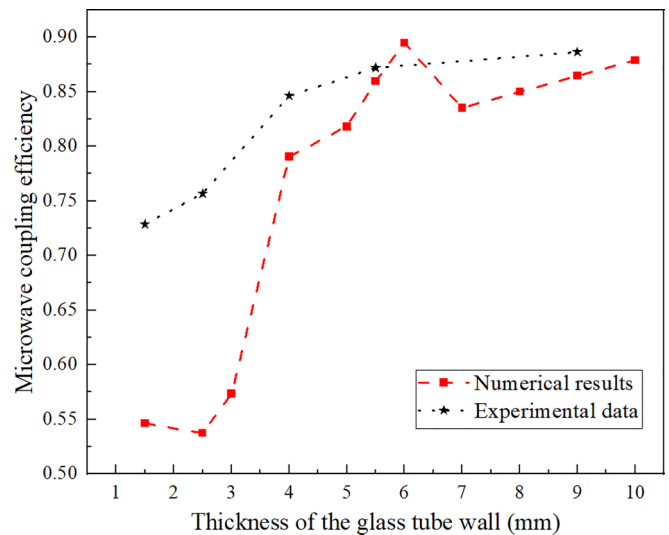

FIG. 8. Effects of the thickness of the glass-tube wall on the microwave power-coupling efficiency and comparison between experimental and numerical results ($P = 1000$ Pa; $P_{in} = 200$ W; and $\varepsilon_g = 3.5$).
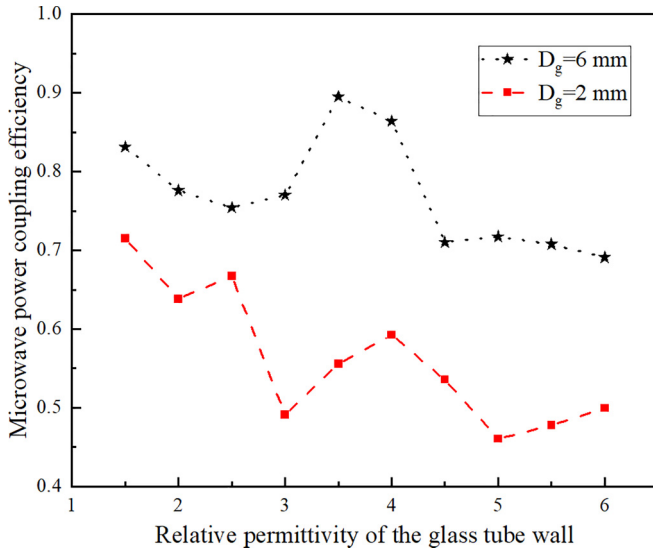
FIG. 9. Effects of the dielectric property of the glass-tube wall on the microwave power-coupling efficiency ($P = 1000$ Pa; and $P_{in} = 200$ W).
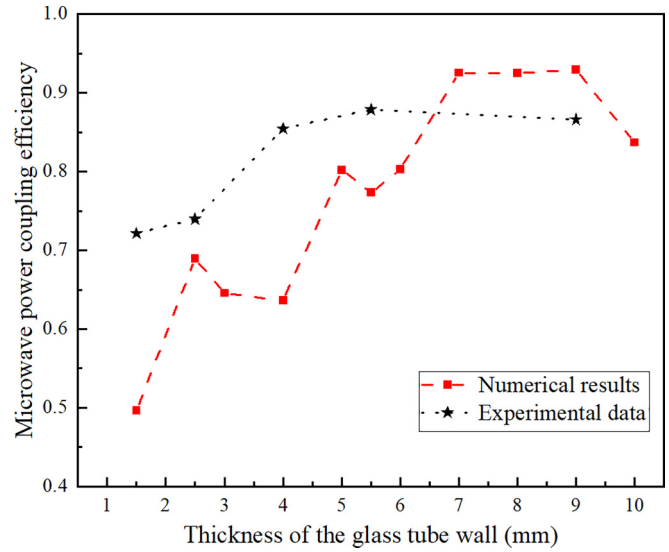

FIG. 10. Effects of the thickness of the glass-tube wall on the microwave power-coupling efficiency and comparison between experimental and numerical results ($P = 500$ Pa; $P_{in} = 200$ W; and $\varepsilon_g = 3.5$).

discharge tube length in the simulations and the scattering boundary conditions mentioned above, the difference may be caused by the following reasons:

(1) The energy-balance equation for the heavy species mixture and the nonlinear couplings with other equations [20–25] were neglected to save computational time and make it acceptable. Consequently, the energy loss due to thermal radiation and nature air-convection cooling was also ignored, which underestimated the microwave coupling efficiency in the calculations.

(2) The gas flow was neglected in the mathematical model, which may have underestimated the numerically obtained energy-coupling efficiency. In experiments, the gas pressure was maintained in a dynamic balance between the argon gas inflow and outflow [28].

(3) The relative permittivity of the quartz glass (ε_g) was set to 3.5, which may not have accorded precisely with experiments. The glass tubes used in our previous experimental study [28] were made of quartz, whose dielectric property depends on the purity of SiO_2, temperature, and microwave frequency [37]. To further explore the effects of the dielectric property of the glass tube on the microwave power-coupling efficiency, more calculations were done, and the results are shown in Fig. 9.

(4) The molecular ions (Ar_2^+) in the argon plasma chemistry and its number density equation in the mathematical model were neglected for a better convergence of the mathematical model.

Figure 10 gives the change of the microwave power-coupling efficiency towards the increase of the thickness of the glass tube under the gas pressure of 500 Pa and the incident microwave power of 200 W. Likewise, the microwave power-coupling efficiency does not increase linearly with the thickness of the glass-tube wall. Nonetheless, the simulated results and the experimental data demonstrate a similar trend that increasing the glass-tube wall's thickness helps improve

the microwave power-coupling efficiency in general, except for some specific values.

Besides the thickness of the glass-tube wall, the material used to make the tube also strongly impacts the traveling-wave propagation characteristics and thereby will further influence the microwave coupling efficiency [27]. It is a much more economical and convenient way to numerically investigate the effects of the dielectric property of the glass-tube wall on the microwave coupling efficiency, compared with customizing a set of tubes with different materials and experimentally measuring it. Figure 9 shows the variation of the microwave coupling efficiency when the relative permittivity of the glass-tube wall increases from 1.5 to 6. In the numerical simulations in Fig. 9, the thickness of the glass-tube wall is set to 2 and 6 mm, corresponding to the thickness most commonly used and the medium thickness of the glass-tube wall, respectively. Figure 9 demonstrates that there is an optimal relative permittivity of the glass-tube wall to achieve the maximum microwave power-coupling efficiency. Besides, both curves in Fig. 9 have shown a similar change tendency that increasing the relative permittivity of the glass-tube wall leads to the decline of the microwave coupling efficiency, although they have some fluctuations.

The results presented in Figs. 8–10 demonstrate that the glass tube, including its wall thickness and dielectric properties, significantly impacts the efficiency of power coupling from the incident microwave to the plasma. The mechanism is the change of impedance matching between the rectangular waveguide and the lossy two-conductor discharge tube consisting of the plasma column and its metallic shielding walls. As is known, the definitions of the voltage and current are not unique for the TE and TM waves in rectangular waveguides [38]. Therefore, the impedance of the TE_{10} mode in rectangular waveguide (Z_e) has three calculation ways: [$Z_e(U-I)$, $Z_e(P-I)$, $Z_e(P-U)$] [39]. However, even using the smallest impedance definition $Z_{e(P-I)} = \frac{\pi^2 b}{8a} Z_{TE10}$

equation, the equivalent impedance of the height-reduced rectangular waveguide part is larger than 100Ω, which is much larger than the impedance of the two-conductor discharge tube. As illustrated above, the discharge tube consisting of the plasma column and its metallic shielding walls can be regarded equivalently as a lossy coaxial waveguide. If further treating the plasma column as a good conductor, the characteristic impedance of the coaxial two-conductor discharge tube (Z_0) in the present study can be defined as follows:

$$Z_0 = \frac{60 \ln \frac{D}{D_p}}{\sqrt{\varepsilon_g}}. \tag{21}$$

$D_p = D - 2D_g$ is the diameter of the plasma column and $D = 30$ mm is the inner diameter of the metallic shielding wall. Even for the largest impedance case ($\varepsilon_g = 1.5$; $D_p = 6$ mm) in the present study, the impedance of the discharge tube is smaller than 100Ω. From the viewpoint of impedance matching ($Z_0 \cong Z_e$), it requires to either increase the thickness of the glass-tube wall or decrease its permittivity. If the impedance of the rectangular waveguide is approximately matched to the coaxial discharge tube, the incident microwave power can enter the discharge tube propagating along the plasma column with little reflection. This is why the glass-tube wall has such a strong impact on the efficiency of power coupling from the incident microwave to the plasma.
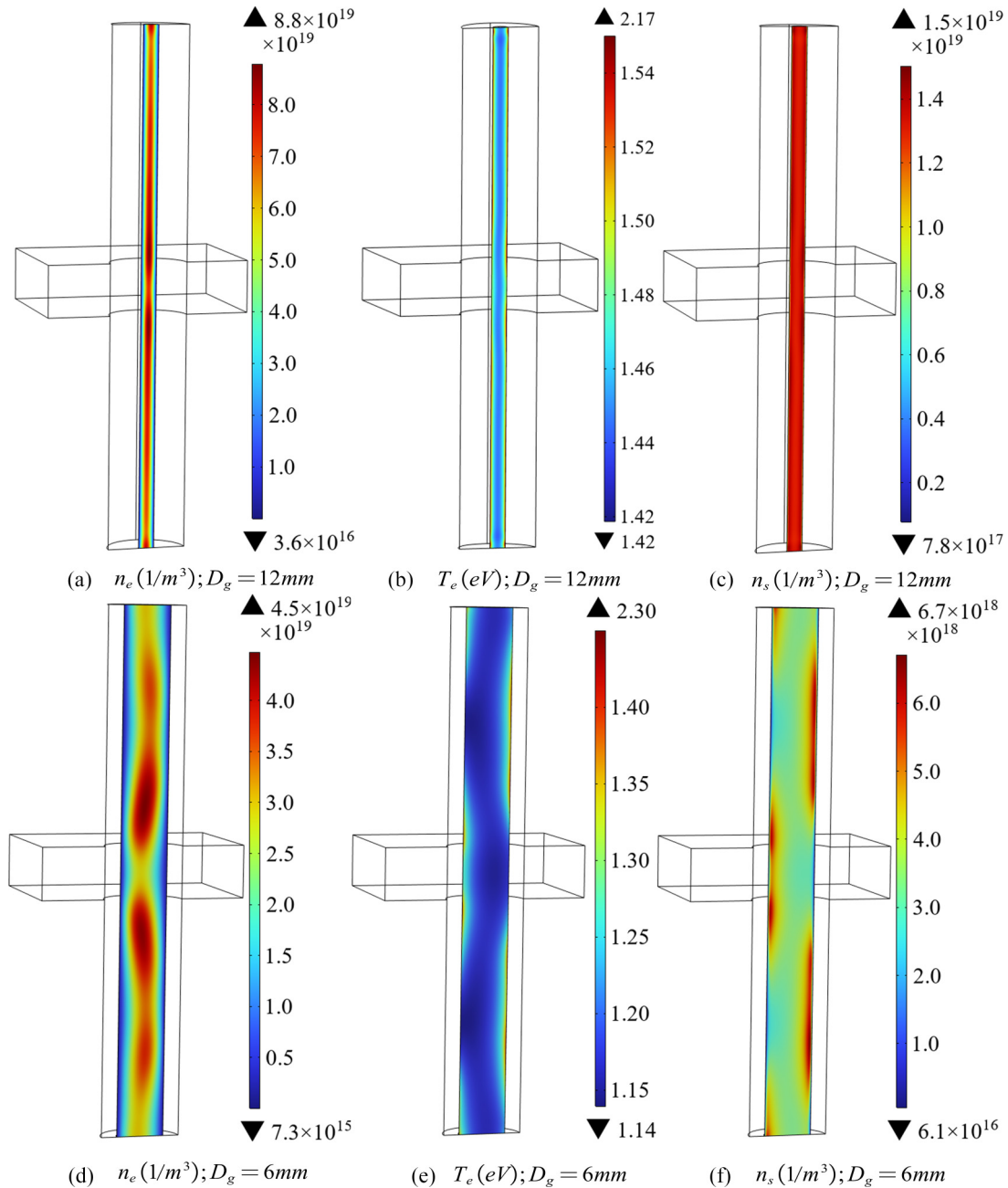

FIG. 11. Distributions of the plasma properties in the glass tubes with different wall thicknesses ($P = 1000$ Pa; $P_{\text{in}} = 200$ W; and $\varepsilon_g = 3.5$).

C. Traveling wave and discharge properties in the MPS with different glass tubes

It has been reported that the electromagnetic modes of the traveling microwave propagating along the plasma can determine the discharge properties to a great extent [40,41]. Figure 6 shows the distributions of the microwave electric fields in the rectangular waveguide part and the cylindrical discharge tube of the MPS. The distribution of the microwave electric field in the discharge is axisymmetric to the axis of the cylindrical discharge tube when the thickness of the glass-tube wall equals 12 mm and the radius of the plasma column is 3 mm. Such a field distribution demonstrates that the electromagnetic mode of the traveling microwave in the discharge tube is the TEM mode. The first-order dominant mode of a coaxial waveguide (TEM mode) can exist in the circular discharge tube because of its waveguide structure transition. If the electron density is high enough, the plasma column and the glass tube with their metallic shielding wall can be equivalently regarded as a two-conductor-like coaxial waveguide that allows the TEM mode to propagate in it.

When the thickness of the glass-tube wall decreases to 6 mm, the distribution of the microwave electric field in the discharge tube becomes nonaxisymmetric. It has one half-wave variation in both the azimuthal direction and the radial direction at the cross section of the discharge tube (if using the cylindrical coordinates), demonstrating that the electromagnetic mode of the traveling wave is TE_{11}. Considering that the first-order mode of the two-conductor waveguide is TEM mode, the traveling microwave in the discharge tube [Fig. 6(b)] propagates in the hybrid TEM and TE_{11} modes. The field distribution mainly presented the characteristics of the TE_{11} mode because the axisymmetric TEM mode was restrained and took a small ratio due to the non-axisymmetric wave excitation for the discharge tube.

Figure 11 shows the distributions of the electron number density, the electron temperature, and the number density of the excited atoms, with different thicknesses of the glass-tube wall ($D_g = 12$ mm and $D_g = 6$ mm). Compared with electromagnetic field distributions in Fig. 6, it proves that the electromagnetic modes of the traveling wave in the discharge tube can decide the discharge properties. When the mode is the axisymmetric TEM, the distributions of the electron number density, the electron temperature, and the number density of the excited atoms become axisymmetric. However, when the mode becomes nonaxisymmetric, the plasma distribution becomes nonaxisymmetric as well.

Figure 7(a) proves that decreasing the dielectric permittivity of the glass-tube wall helps eliminate the higher-order electromagnetic modes and maintain only the TEM mode in the discharge tube. Figure 7(b) shows the effects of changing the glass-tube wall's dielectric permittivity on the discharge properties. The plasma distribution becomes axisymmetric, corresponding to the axisymmetry of the sustaining microwave. The above conclusions drawn from Fig. 7 are from multiphysics modelings that have taken the gas-discharge process and the plasma sustaining into simulations. The results are definitely quite representative of reality compared to those from the full-wave electromagnetic analysis in our previous study [27], where the plasma was assumed with a preset electron number density and a constant electron collision frequency for simplicity. Nevertheless, the findings of our present and previous studies concur in demonstrating that changing the dielectric permittivity (material) of the glass-tube wall can alter the electromagnetic modes of the traveling microwave propagating along the plasma column.

IV. CONCLUSION

This study has proposed a transient three-dimensional model to simulate the microwave propagation and the argon discharge in a waveguide-based MPS under intermediate pressures. A plane-symmetric simplification based on the characteristic of the microwave field distributions in the MPS was used to simplify the computational domain and reduce the calculation time. The entire discharge process from 1×10^{-9} to 1×10^4 s was simulated, which covered the instantaneous microwave breakdown to the formation of a stable plasma column near steady state. The results revealed the waveguide structure transition of the MPS and the consequent microwave distribution variation in the discharge process. A series of efficiencies of power coupling from the incident microwave to the plasma at 1×10^4 s was calculated under different operation conditions (pressures and glass tubes) and compared with the experimental data. The electromagnetic modes of the traveling wave in the discharge tube were analyzed and compared with our previous study. These comparisons demonstrated the validity of the mathematical model and the plane-symmetric simplification. The validity indicates the plane-symmetric simplification method can be extended to model other types of MPSs on the condition that the microwave electric field exhibits plane symmetry. Besides, the obtained conclusions regarding the effects of the glass tube on the microwave power-coupling efficiency and the electromagnetic modes can provide references to the design of other MPS configurations. These effects can be summarized as follows:

(1) Increasing the thickness of the glass-tube wall helps improve the power-coupling efficiency from the incident microwave to the plasma. In contrast, increasing the permittivity of the glass-tube wall generally leads to the decline of the microwave coupling efficiency. This phenomenon occurs because increasing the wall thickness of the glass tube or reducing its permittivity enhances the impedance matching between the two-conductor discharge tube and the rectangular waveguide, thus facilitating a more efficient energy transfer.

(2) The higher-order nonaxisymmetric electromagnetic modes can be restrained by increasing the glass-tube wall's thickness or decreasing its permittivity. This is attributed to the cutoff-frequency limitation of the TE_{11} mode within the coaxial two-conductor waveguide structure of the discharge tube [27,38]. As the plasma radius and the permittivity of the glass-tube wall decrease, the cutoff frequency increases, supressing the incident microwave at the frequency of 2.45 GHz to propagate in nonaxisymmetric TE_{11} mode.

(3) The electromagnetic modes of the traveling microwave that sustains the discharge in the MPS have a strong influence on the plasma distribution. When the electromagnetic mode of the traveling microwave is axisymmetric, the plasma also becomes axisymmetric. When the higher-order nonaxisymmetric electromagnetic modes are excited, the plasma parameters will also become nonaxisymmetric.

However, it is worth noting that the above conclusions are drawn particularly for the waveguide-based MPS with a 30-mm-diameter cylindrical metallic enclosure confining the glass tube. Besides, to reduce the nonlinear couplings between each equation and the calculation time, making it possible for the complicated multiphysics model to be solved in three dimensions within an acceptable time, the heat-transfer equation for the heavy species and the molecular ions Ar_2^+ in plasma chemistry are neglected, which will introduce errors to the numerical simulations. These factors, together with the difference between experiments and modelings in the glass-tube wall's dielectric permittivity, are the reasons why some calculated microwave coupling efficiencies in the present study do not agree ideally with the experimental data. Therefore, an improved model considering more particle species, physical processes, and couplings between each equation is needed, which will be our future work.

[1] M. Moisan, Z. Zakrzewski, R. Pantel and P. Leprince, IEEE Trans. Plasma Sci. **PS-12**, 203 (1984).

[2] H. S. Uhm, Y. C. Hong and D. H. Shin, Plasma Sources Sci. Technol. **15**, S26 (2006).

[3] M. Moisan, C. Beaudry, and P. Leprince, IEEE Trans. Plasma Sci. **PS-3**, 55 (1975).

[4] Q. H. Jin, C. Zhu, M. W. Border, and G. M. Hieftje, Spectrochim. Acta. Part B: At. Spectrosc. **46**, 417 (1991).

[5] R. Miotk, M. Jasinski, and J. Mizeraczyk, IEEE Trans. Microw. Theory Technol. **66**, 711 (2018).

[6] A. I. Al-Shamma'a, S. R. Wylie, J. Lucas, and C. F. Pau, J. Phys. D: Appl. Phys. **34**, 2734 (2001).

[7] J. H. Kim, Y. C. Hong, and H. S. Uhm, Surf. Coat. Technol. **201**, 5114 (2007).

[8] R. Rincon, A. Marinas, J. Munoz, and M. D. Calzada, Chem. Eng. J. **284**, 1117 (2016).

[9] B. Hrycak, D. Czylkowski, R. Miotk, M. Dors, M. Jasinski, and J. Mizeraczyk, Int. J. Hydrogen Energy **39**, 14184 (2014).

[10] N. Bundaleska, D. Tsyganov, R. Saavedra, E. Tatarova, F. M. Dias, and C. M. Ferreira, Int. J. Hydrogen Energy **38**, 9145 (2013).

[11] G. Chen, T. Silva, V. Georgieva, T. Godfroid, N. Britun, R. Snyders, and M. P. Delplancke-Ogletree, Int. J. Hydrogen Energy **40**, 3789 (2015).

[12] G. Chen, N. Britun, T. Godfroid, V. Georgieva, R. Snyders, and M. P. Delplancke-Ogletree, J. Phys. D: Appl. Phys. **50**, 084001 (2017).

[13] H. S. Uhm, H. S. Kwak, and Y. C. Hong, Environ. Pollut. **211**, 191 (2016).

[14] R. Snoeckx and A. Bogaerts, Chem. Soc. Rev. **46**, 5805 (2017).

[15] T. Silva, N. Britun, T. Godfroid, and R. Snyders, Plasma Sources Sci. Technol. **23**, 025009 (2014).

[16] G. S. J. Sturm, A. N. Muñoz, P. V. Aravind, and G. D. Stefanidis, IEEE Trans. Plasma Sci. **44**, 670 (2016).

[17] A. Sanlisoy and M. O. Carpinlioglu, Int. J. Hydrogen Energy **42**, 1361 (2017).

[18] V. J. Dijk, K. Peerenboom, M. Jimenez, D. Mihailova, and J. V. D. Mullen, J. Phys. D: Appl. Phys. **42**, 194012 (2009).

[19] V. J. Dijk, G. M. W. Kroesen, and A. Bogaerts, J. Phys. D: Appl. Phys. **42**, 190301 (2009).

[20] Y. Kabouzi, D. B. Graves, E. Castaños-Martínez, and M. Moisan, Phys. Rev. E **75**, 016402 (2007).

[21] J. Henriques, E. Tatarova, and C. M. Ferreira, J. Appl. Phys. **109**, 023301 (2011).

[22] H. Nowakowska, M. Jasinski, and J. Mizeraczyk, Eur. Phys. J. D **67**, 133 (2013).

[23] V. Georgieva, A. Berthelot, T. Silva, S. Kolev, W. Graef, N. Britun, G. X. Chen, J. van der Mullen, T. Godfroid, D. Mihailova, V. J. Dijk, R. Snyders, A. Bogaerts, and M.-P. Delplancke-Ogletree, Plasma Process Polym. **14**, 1600185 (2016).

[24] M. Baeva, F. Hempe, H. Baierl, T. Trautvetter, R. Foestand, and D. Loffhagen, J. Phys. D: Appl. Phys. **51**, 385202 (2018).

[25] W. C. Zhang, J. W. Tao, K. M. Huang, and L. Wu, IEEE Trans. Plasma Sci. **45**, 2929 (2017).

[26] W. C. Zhang, L. Wu, J. W. Tao, and K. M. Huang, IEEE Trans. Plasma Sci. **47**, 271 (2019).

[27] W. C. Zhang, L. Wu, K. M. Huang, and J. W. Tao, Phys. Plasmas. **26**, 042101 (2019).

[28] W. C. Zhang, L. Wu, Z. Liu, J. W. Tao, and K. M. Huang, Phys. Plasmas. **27**, 033510 (2020).

[29] M. Koshiba, K. Hayata, and M. Suzuki, IEEE Trans. Microwave Theory Tech. **33**, 227 (1985).

[30] M. A. Lieberman and A. J. Lichtenberg, *Principles of Plasma Discharges and Materials Processing* (Wiley, New York, 2005).

[31] D. P. Lymberopoulos and D. J. Economou, J. Appl. Phys. **73**, 3668 (1993).

[32] K. Makasheva and A. Shivarova, Phys. Plasmas **8**, 836 (2001).

[33] M. Baeva, A. Bösel, J. Ehlbeck, and D. Loffhagen, Phys. Rev. E **85**, 056404 (2012).

[34] R. Q. Liu, Y. Liu, W. Z. Jia, and Y. W. Zhou, Phys. Plasmas **24**, 013517 (2017).

[35] Y. P. Raizer, *Gas Discharge Physics* (Springer, Berlin, 1997).

[36] F. Z. Wei, H. X. Wang, A. B. Murphy, W. P. Sun, and Y. Liu, J. Phys. D: Appl. Phys. **46**, 505205 (2013).

[37] M. R. Stuart, J. Appl. Phys. **26**, 1399 (1955).

[38] D. M. Pozar, *Microwave Engineering*, 4th ed. (Wiley, Hoboken, 2005).

[39] J. Helszajin, *Ridge Waveguides and Passive Microwave Components* (IET, London, 2000).

[40] E. Benova and I. Zhelyazkov, Phys. Scr. **56**, 381 (1997).

[41] M. Moisan and H. Nowakowska, Plasma Sources Sci. Technol. **27**, 073001 (2018).